# Design and Control of a Low-Cost EMG-Based Soft Robotic Ankle-Foot Orthosis for Foot Drop Rehabilitation

**Nitish Gudapati, Koushik Kumaran, S. V. Deepak, R. Mukesh Kanna, R. Jinesh, and Himadri Poddar**

**Abstract** Stroke patients often suffer from foot drop, a gait abnormality caused due to the paralysis of the anterior portion muscles of the lower leg, causing an inability or impaired ability to raise the foot at the ankle joint. This condition leads to extremities of the foot being dragged along the ground while walking, causing tripping and other accidents. Braces or splints that fit into shoes are prescribed to help hold the foot in a normal position. For rehabilitation, most patients are trained to walk with canes, and therapists prescribe physiotherapy for a series of short, intensive sessions. These solutions are expensive and slow processes as they require the presence of skilled personnel. In this paper, we present a novel design and control methodology for a 1-DoF Soft Active Ankle-Foot Orthosis (AFO) to address these issues. The AFO is designed to augment the human musculoskeletal system. The AFO is actuated using McKibben muscles (pneumatic artificial muscles), which are driven pneumatically. They are cost-effective and lightweight, offering a significant advantage over motor-driven orthoses. The orthosis is controlled using electromyography (EMG) signals from the muscles involved in the motion of the ankle. The use of EMG for control is found to be a better option than existing methods due to its non-invasive nature.

**Keywords** Active foot orthosis · Electromyography (EMG) · Foot drop · Rehabilitation · Soft robotics

## 1 Introduction

According to the World Health Organization, 15 million people suffer stroke worldwide each year. Of these, 5 million people die, and another 5 million are permanently disabled [1]. A common ailment for stroke survivors is foot drop, i.e., the inability to actively perform Dorsiflexion of the foot. This leads to the occurrence of steppage

Supported by Institute grants through the Robotics and Machine Intelligence Club, NIT Tiruchirappalli, INDIA.

N. Gudapati (✉) · K. Kumaran · S. V. Deepak · R. Mukesh Kanna · R. Jinesh · H. Poddar
National Institute of Technology, Tiruchirappalli, Tamil Nadu 620015, India



R. Kumar et al. (eds.), *Machines, Mechanism and Robotics*, Lecture Notes in Mechanical Engineering, https://doi.org/10.1007/978-981-16-0550-5_130

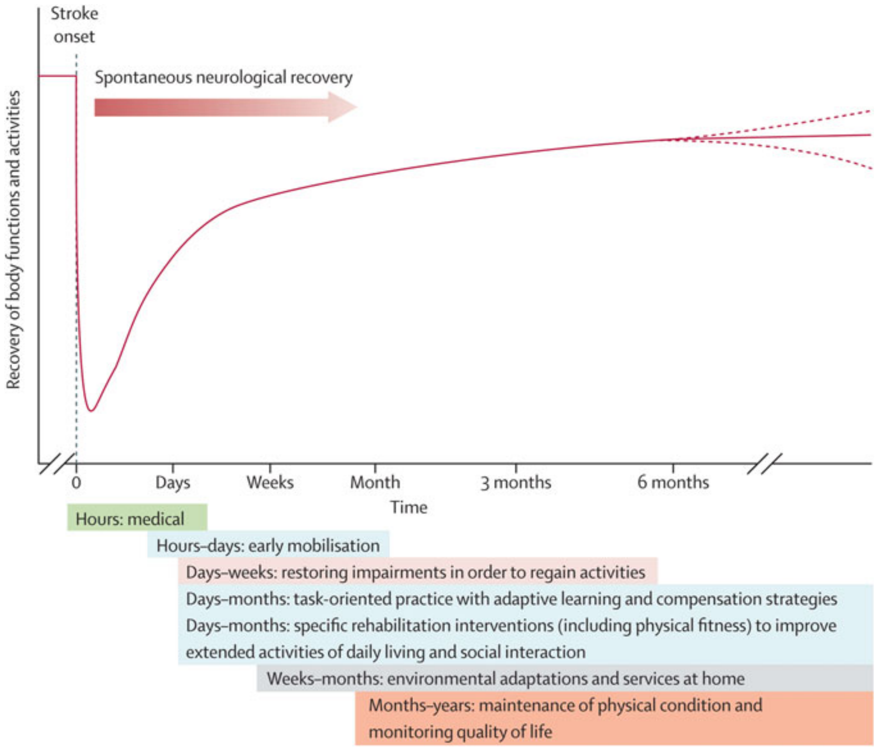


**Fig. 1** Hypothetical pattern of recovery after stroke with the timing of intervention strategies. *Source* [4]

gait, where the foot drags along, requiring the patient to raise their knee higher than usual in the swing phase to counter this [2]. The patient's foot slaps the ground during the foot strike phase of the gait cycle. Studies have shown that the entire kinematic chain of the lower body is disturbed, resulting in the functioning of the motor system under abnormal load [3]. Patients generally undergo therapy to regain motor control, and the required recovery can take from months to years to complete as shown in Fig. 1 [4]. The available number of medical professionals is far less than the requirement, and they may not be accessible to all those who need it [5]. To this end, robotic devices can significantly decrease the burden on therapists and caregivers and can be used to provide intensive task-oriented practice.

Considerable research has gone into developing such robotic devices, especially for upper-body rehabilitation [6–8]. Most of these devices, however, are rigid, heavy and unwieldy. In recent years, the interest in a compliant robotic system has increased exponentially, due to the significant advantages they provide. McKibben muscles or pneumatic artificial muscles (PAM) are a possible actuation method with properties that make them uniquely suited for the application presented. These properties are explored in depth in Sect. 4.

In this paper, we describe the design and control of a single DOF orthosis, actuated with PAMs and controlled with electromyography (EMG) signals. The EMG sensors are non-invasive, and the design of the orthosis is compliant, lightweight and wearable. Section 2 explains the practices and techniques involved in the rehabilitation of the foot and Sect. 3 explains the existing orthoses and exoskeletons for foot rehabilitation. Section 4 discusses the construction and working of the prototype, and the results are presented in Sect. 5. Some concluding remarks and future scope are mentioned in Sect. 6.

## 2 Rehabilitation Techniques

To understand the requirements and specifications of stroke rehabilitation devices, a brief introduction of common existing techniques is given below [9].

### *2.1 Physiotherapy*

The primary technique used is physiotherapy which involves assessment of a physiotherapist using various techniques. The techniques include various exercises.
**Mobility training** is done to stabilize and strengthen to enhance balance and support.
**Range of Motion Therapy** helps in easing muscle tension allowing a good range of motion.

### *2.2 Technology-Assisted*

**Functional Electrical Stimulation** method involves inducing contraction to the weak muscles by application of electricity which helps in training them.

**Game System Technology** is based on the idea of integration of games for rehabilitation. They involve functional activities and keep the patient occupied and motivated with games during the rehabilitation process.

## 3 Existing Technologies for Rehabilitation

Robotic exoskeletons have been employed in assisting individuals suffering from physical disability either for the advancement of therapy or as a permanent assistive tool. They are of various types and can be classified based on their method of actuation. **Rigid actuation** devices are actuated using DC motors, steppers, etc. **Soft**

**actuation** devices are actuated using compliant methods which generally include pneumatic or using shape memory alloys (SMA) [10–13]. The AFO described in this paper falls under this category.

### *3.1 Rigid Actuation*

**Anklebot at Massachusetts Institute of Technology (MIT), USA** The Anklebot is a 3-DOF wearable robot, which is actuated using two BLDC motors. The linear actuators are mounted in parallel and provide actuation in two of the ankle's 3-DOF [14]. Position information is provided by encoders.

**ALEX at University of Delaware, USA** This exoskeleton is mounted with a walker to support the device. The controller applies a force-field at the ankle of the subject providing the necessary torque to move it [15]. The disadvantage is that it is not easily portable.

### *3.2 Soft Actuation*

**Wearable Soft Exoskeleton at Carnegie Mellon University, USA** The exoskeleton uses four PAMs connected to the knee and foot braces with the help of artificial tendons [11]. It helps with therapy, but it does not provide much independence for the user.

**Powered Ankle-Foot Orthosis at University of Michigan, USA** This orthosis is actuated by PAMs providing only plantar flexion torque. It uses a real-time computer interface for controlling the air pressure supplied to the PAMs which is determined using a footswitch placed under the foot [12].

**Adaptive Control of Actuated Ankle-Foot Orthosis (AAFO) at Paris-Est Créteil University, France** AAFO uses a predetermined trajectory of the ankle's swing phase of the gait cycle, to provide the required assistance [13].

## 4 Construction and Working

### *4.1 Design of the Prototype*

The design of the AFO focuses on achieving the following goals:

- User comfort
- Minimal weight
- Complete range of motion about a single axis

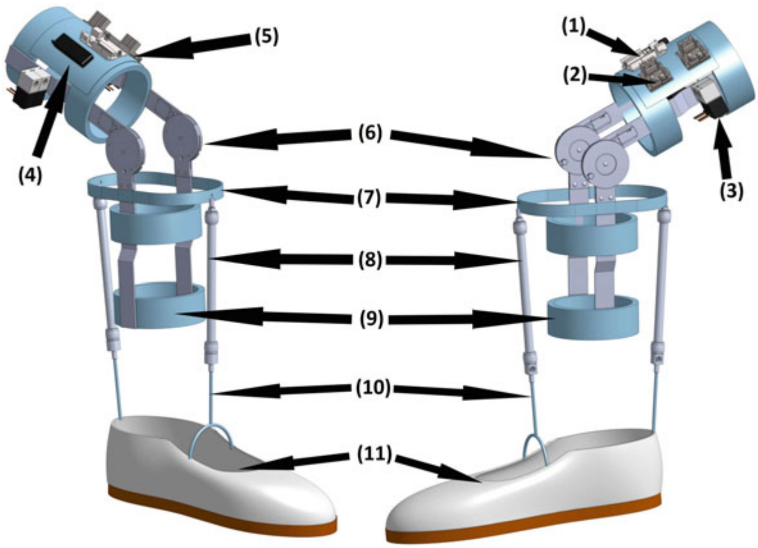


**Fig. 2** AFO's Layout. Components labelled from (1) to (11): (1) Arduino Uno; (2) motor drivers; (3) solenoid valves; (4) Li-Po; (5) panel for electronic circuitry; (6) knee braces; (7) PAM mount; (8) PAM; (9) foam padding; (10) adjustable strings; (11) orthotic sole

- Simple setup
- Minimal cost.

**Pneumatic Artificial Muscle Design** Each PAM consists of a silicone rubber tube, placed within a nylon mesh sleeve. One end is pneumatically sealed, and the other end is used as an inlet for pressurized air. When air flows into the tube, it expands volumetrically. Since the sleeve's structure only allows it to expand radially while contracting longitudinally, the PAM contracts when pressurized.

Multiple studies have been performed on these PAMs, and the force-length characteristics are found to be similar to that of a muscle [16]. The materials used in the PAM are compliant, lightweight and low-cost, making them well suited for the AFO.

The analysis of various characteristics of the PAM is presented in Sect. 5. The required length, diameter and pressure of the PAM were decided upon through experiments with various configurations, presented in Sect. 5.

**Orthosis Design**

The computer-aided design of the prototype is presented in Fig. 2. The orthosis consists of thigh and shin supports connected by a knee brace or a hinge joint which offers full range of motion of the knee. This framework along with the shin of the leg acts as the ground link for the actuating mechanism. The sole attached to the foot is the end effector which can be modelled as hinged at the shin.

The knee brace and the sole are connected using two PAMs in an agonist-antagonist configuration, each one providing the necessary dorsiflexion and plantarflexion forces, respectively. The point of the PAM hinged to the sole is dependant

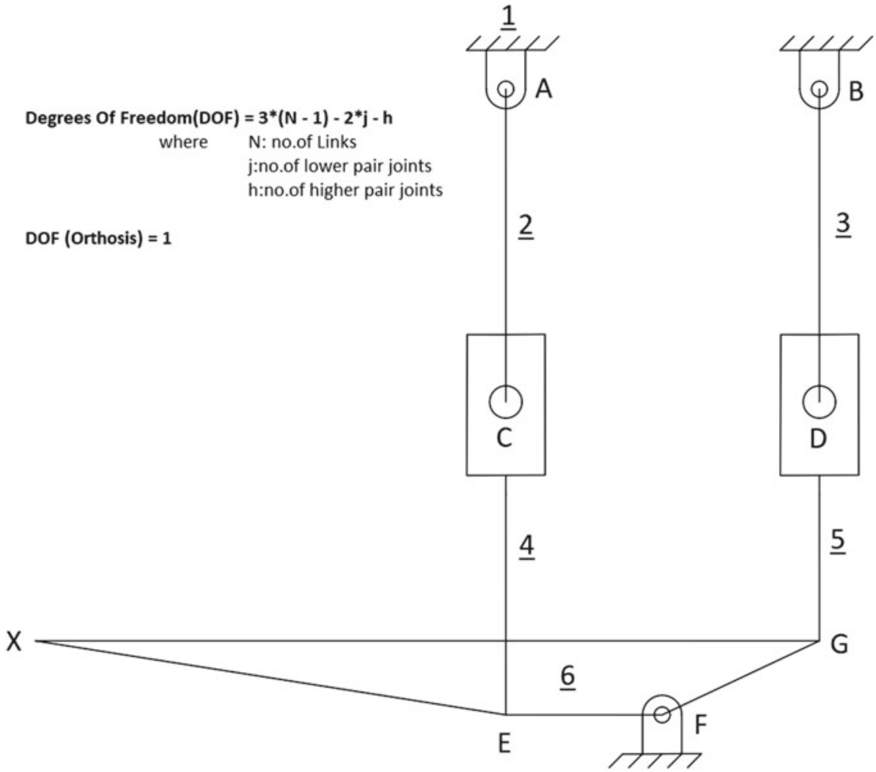


**Fig. 3** Kinematic model of the orthosis

on the required actuation torque and range of motion. Since PAMs are shown to provide a good amount of force [16], but only limited contraction, the choice was made to place them very close to the joint and the length of the force arm was determined experimentally as 3 cm. The corresponding data is presented in Sect. 5. This allows the AFO to achieve the entire Range of Motion which is roughly 20° for dorsiflexion and 50° for plantarflexion [17].

Some similar devices [18, 19] have been constructed with the ground at the shin, connected to the ankle end effector in a similar fashion. We found that in this configuration, the transverse reaction forces during PAM contraction resulted in skin deformation at the skin-AFO interface causing user discomfort and restriction in the range of motion of the AFO. By placing additional support above the knee, the reaction force is made almost normal to the skin-AFO interface, thereby providing good support with no loss in user comfort. Figure 3 presents the kinematic model of the designed orthosis along with the degrees of freedom of actuation that the orthosis provides.

**Electronics and Pneumatic Circuitry** Each PAM is controlled by a pair of 2-position 2-way solenoid valves, where one acts as an inlet and the other acts as an outlet. Each pair of valves is connected to an MCU and an L298N Driver for power

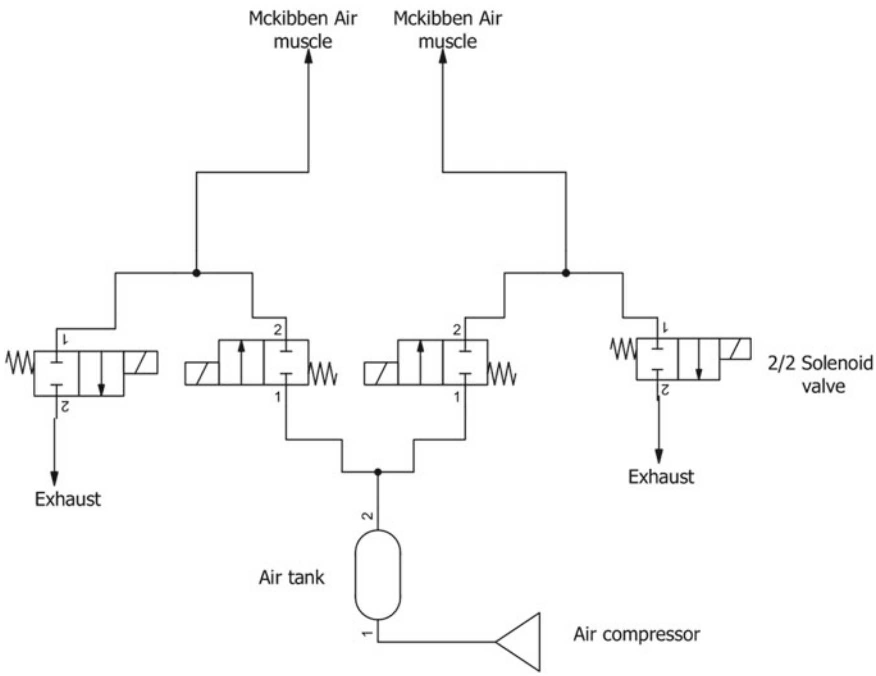


**Fig. 4** Pneumatic circuit

and logic. Two MyoWare EMG sensors are connected to the same MCU. The entire setup is powered by a 12V lithium-polymer battery and placed above the knee to optimize weight distribution throughout the AFO.

Both the inlet valves are connected to an air tank with pressurized air at 45 PSI, and the exhaust valves are left open to the atmosphere as shown in Fig. 4. All pneumatic connections were made with 8 mm OD $\times$ 6 mm OD polyurethane pneumatic tubes. The control methodologies for the PAMs are described in Sect. 4.2.

## *4.2 Control of the Orthosis*

**Signal Acquisition** In order to detect the intent of the user, the AFO uses MyoWare muscle sensors and EMG electrodes. Each McKibben muscle is placed so as to assist the functioning of a specific muscle. The targeted muscles are:

- Tibialis anterior for dorsiflexion
- Soleus for plantarflexion.

The positions of these muscles are depicted in Fig. 5.

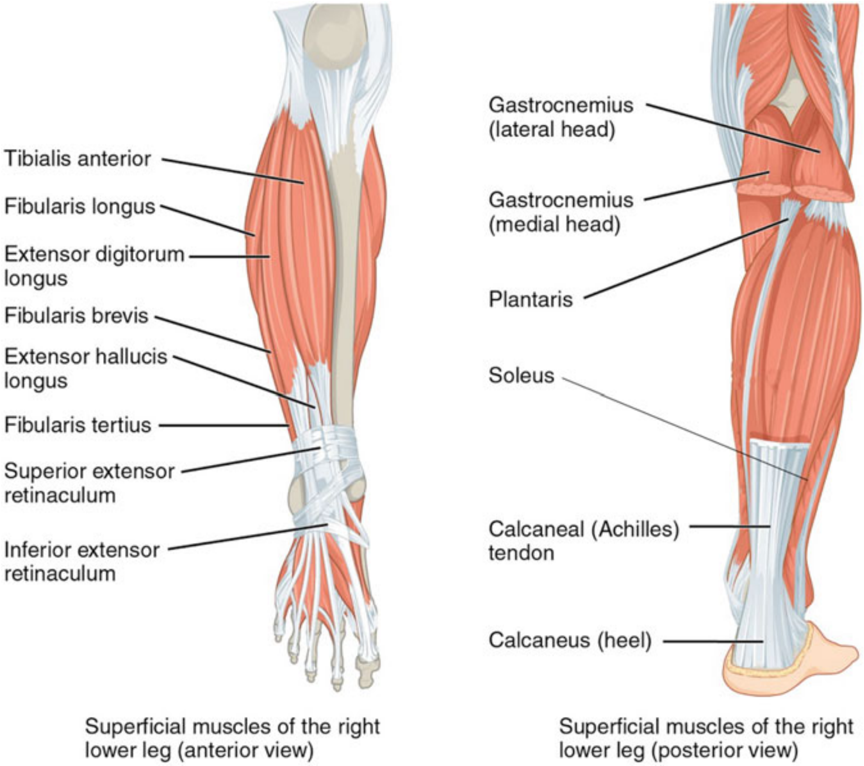


**Fig. 5** Muscles of the leg. *Source* [20]

Each muscle requires a non-invasive EMG sensor and each sensor requires the placement of three electrodes to capture the differential component of the signal travelling across the muscle. As per EMG electrode placement standards [21], one electrode is placed near the centre of a muscle, one electrode near the end of a muscle and a ground electrode is placed near a bone for reference. The rectified and integrated signal is sampled by the 10-bit ADC of the MCU at a rate 200 Hz.

**EMG Analysis** The rectified and integrated signals (signal envelopes) from the MyoWare muscle sensors produce output with added noise. Studies show that the noise from sEMG signal includes both high frequency components and low frequency components arising from movement artefacts [22]. To overcome this, the signals from both EMG sensors were passed to two independent 1-dimensional Kalman filters. Due to the difficulty involved in creating a dynamic model, a linear predictive model was used, where the filtered output from the previous iteration was taken as the initial estimate for the next iteration. It was found that a value of 0.001 for process noise covariance gave the best results for both sensors while inducing only negligible latency in the filtered output as shown in Fig. 6.

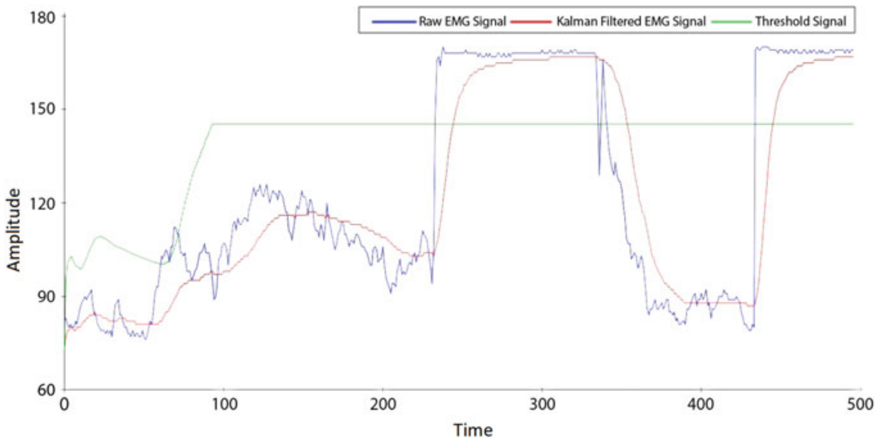


**Fig. 6** EMG signal acquisition, filtering and thresholding

EMG signals for a muscle are highly dependent on a multitude of factors such as electrode placement, fatigue, and the physical and mental state of the user and other EMG artefacts [23, 24]. Hence, real-time calibration is done before every session. This happens automatically on initialization of the AFO. This calibration procedure sets the threshold for each muscle to enable intent estimation, which is described below. This also addresses the issues due to EMG degradation by adjusting the threshold.

The rest state characteristics of each muscle are obtained by recording the unfiltered EMG envelope for 10 s. The mean ($\mu_{\text{rest}}$) and standard deviation ($\sigma_{\text{rest}}$) of this data are extracted from this data. Using the collected data, a threshold is calculated for each target muscle using Eq. (1) for dorsiflexion and Eq. (2) for plantarflexion. This threshold is then used to detect activation of each muscle. The muscle is found to be actively contracting when the filtered signal exceeds the threshold.

For tibialis anterior muscle, the threshold is determined by Eq. (1),

$$T = \mu_{\text{rest}} + 3 * \sigma_{\text{rest}} \tag{1}$$

For soleus muscle, the threshold is determined by Eq. (2),

$$T = \mu_{\text{rest}} + 8 * \sigma_{\text{rest}} \tag{2}$$

Studies have shown that a threshold equal to the mean added to a multiple of the standard deviation gives accurate results when applied to the EMG envelope [25]. The values of the constant multiplier for standard deviation were determined experimentally. The accuracy of intent detection with these values was tested and the results are described in Sect. 5.

**Intent Detection Logic** Using the described method, we determine the state of a muscle in real time. It was determined that the soleus muscle was active during plan-

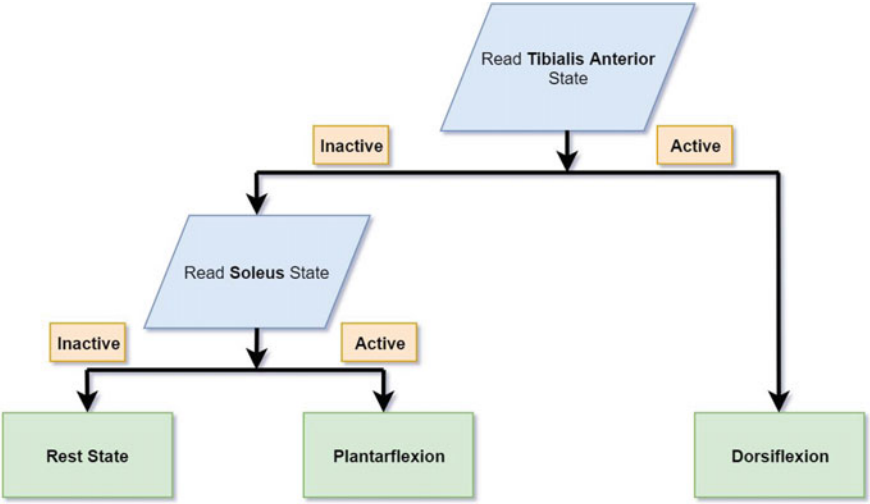


**Fig. 7** Intent detection

**Table 1** State of solenoid valves

| PAM movement | Inlet valve | Exhaust valve |
|---|---|---|
| Relax (Deflate) | Close | Open |
| Contract (Inflate) | Open | Close |

tarflexion, and the initial and final stages of dorsiflexion. This is visualized in Fig. 10, which shows plantarflexion, followed by dorsiflexion. Using this information, user intent is detected by the method specified in Fig. 7.

## Control of PAM with EMG

The user closes the feedback loop by attempting to move their ankle by muscle contraction. This eliminates the need of external feedback and allows real-time intent detection.

In order to contract a PAM, pressurized air is inflated into it by opening the inlet valve and by closing the outlet valve. In order to relax (expand) a PAM, the air inside it is exhausted by closing the inlet valve and opening the outlet valve. Table 1 summarizes the valve positions for different PAM configurations.

In order to ensure smooth movement of the foot, the speed of inflation or deflation of the PAMs is reduced by applying a pulse width modulated (PWM) signal to the valves. Through experiments, it was found that a PWM signal with a time period of half a second and a duty cycle of 10% for 5 s was ideal. The duty cycle can be modified to provide varying angular velocities. Figure 8 depicts the operation of the AFO. The AFO is an open-loop system; however, the user closes the control-loop while using the orthosis. This make the device simple, efficient and cost-effective.

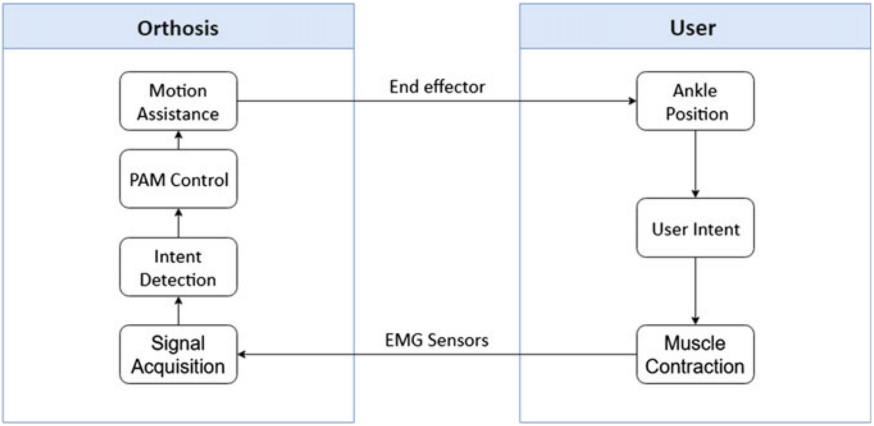


**Fig. 8** Operation flowchart

**Table 2** State of pneumatic artificial muscles

| Intent | Dorsiflexor PAM | Plantarflexor PAM |
|---|---|---|
| Rest state | Relax | Relax |
| Plantarflexion | Relax | Contract |
| Dorsiflexion | Contract | Relax |

After detecting user intent, control signals from the MCU are sent to the LM298 drivers that control the pneumatic valves. Table 2 describes the state of each PAM with respect to various user inputs.

# 5 Results and Statistical Data

## *5.1 Pneumatic Artificial Muscles Tests*

The PAMs were tested on an experimental setup consisting of a rigid support to attach the actuator. The other ends of the PAMs were attached to a pan to test contraction under varying loads. The PAMs were connected to an air compressor maintained at a constant pressure while testing. A vernier scale was fixed along the length of the PAM.

Initially, PAMs of different lengths and diameters were tested to determine the combination that provides maximum percentage contraction under a minimal load of 1 kg and 45 PSI pressure. These results are presented in Table 3. PAM of 30 cm length with an inner diameter of 1/3 in. was found to be optimal due to its percentage contraction and satisfying the length constraints of the average leg.

**Table 3** Pneumatic artificial muscles tests

| Inner diameter (inches) | Outer diameter (inches) | Length of muscle (cm) | Length contraction (cm) | Percentage contraction (%) |
|---|---|---|---|---|
| 1/3 | 1/2 | 20 | 2.5 | 12.5 |
| 1/2 | 5/8 | 20 | 1.8 | 9.0 |
| 1/3 | 1/2 | 30 | 5.1 | 17.0 |
| 1/2 | 5/8 | 30 | 3.0 | 10.0 |

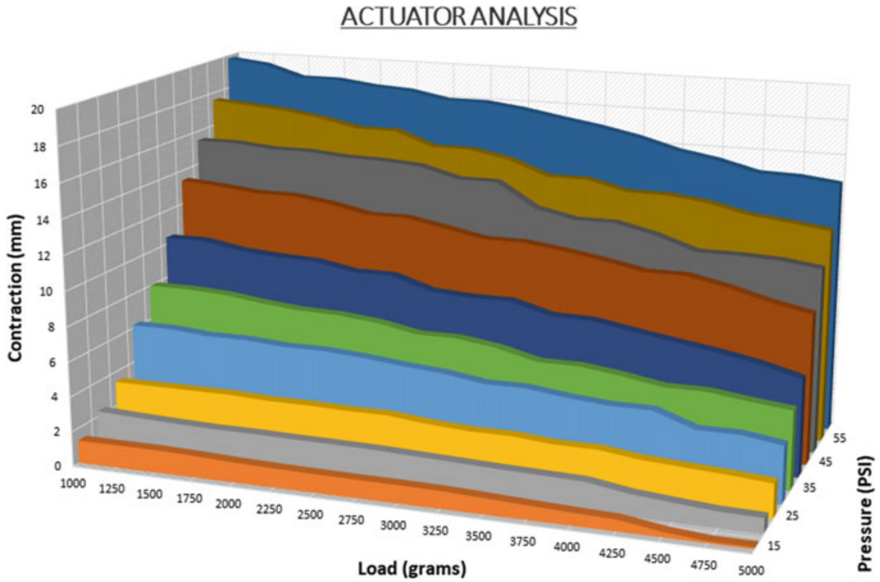


**Fig. 9** Pressure-contraction-load analysis of the PAM designed

Once the PAM characteristics were decided, the length of the force arm was determined by testing the contraction of the PAM under various pressures and loads in the abovementioned experimental setup. This data is presented in Fig. 9. The length of force arm was selected as 3 cm by taking into account the maximum pressure of the tank and the load borne by the actuator, and the required range of motion which is 20° for dorsiflexion, 50° for plantarflexion [17].

## 5.2 *EMG Control Tests*

The AFO was tested by three of the authors as the particants for the study. The participants flexed their legs over the entire range of motion for both dorsiflexion and plantarflexion, and the percentage accuracy of intent detection in every case

**Table 4** Participants were relaxed

| Participant | Dorsiflexion (%) | | | Plantarflexion (%) | | |
|---|---|---|---|---|---|---|
| | Accuracy | False-positive | False-negative | Accuracy | False-positive | False-negative |
| 1 | 95.00 | 1.67 | 3.33 | 90.00 | 1.67 | 8.33 |
| 2 | 100.00 | 0.00 | 0.00 | 98.33 | 0.00 | 1.67 |
| 3 | 96.67 | 1.67 | 1.67 | 91.67 | 1.67 | 6.67 |

**Table 5** Participants were fatigued

| Participant | Dorsiflexion (%) | | | Plantarflexion (%) | | |
|---|---|---|---|---|---|---|
| | Accuracy | False-positive | False-negative | Accuracy | False-positive | False-negative |
| 1 | 90.00 | 1.67 | 8.33 | 90.00 | 3.33 | 6.67 |
| 2 | 95.00 | 1.67 | 3.33 | 91.67 | 3.33 | 5.00 |
| 3 | 91.67 | 3.33 | 5.00 | 90.00 | 5.00 | 5.00 |

was calculated and presented. Table 4 presents the data when they were relaxed and Table 5 after a while when fatigued.

The control scheme achieves a mean dorsiflexor accuracy of 97.22% and inaccuracies being 1.11% false-positive and 1.67% false-negative. The mean plantarflexion accuracy is 93.33%, and the inaccuracies are 1.11% false-positive and 5.56% false-negative.

The control scheme achieves a mean dorsiflexor accuracy of 92.22% and inaccuracies being 2.22% false-positive and 5.56% false-negative. The mean plantarflexion accuracy is 90.56% and the inaccuracies are 3.88% false-positive and 5.56% false-negative.

From the results mentioned in Tables 4 and 5, it is found that the simple control scheme presented is able to achieve a mean dorsiflexion accuracy of 94.72%, and inaccuracies being 1.66% false-positive and 3.62% false-negative. The mean plantarflexion accuracy is 91.94% and the inaccuracies are 2.5% false-positive and 5.56% false-negative. It is worth noting that the accuracy decreases minimally when the participants are fatigued.

**Performance** The orthosis exhibited a good response time to the changes in the EMG-based muscle activation signal with minimal lag due to the simple control logic. The absence of a feedback control signal also eliminates the time delay introduced by sensors and error detectors. The activation function's output for both the muscles is shown in Fig. 10. An ergonomic and compliant prototype of the orthosis was made as a proof of concept. The completed prototype is shown in Fig. 11.

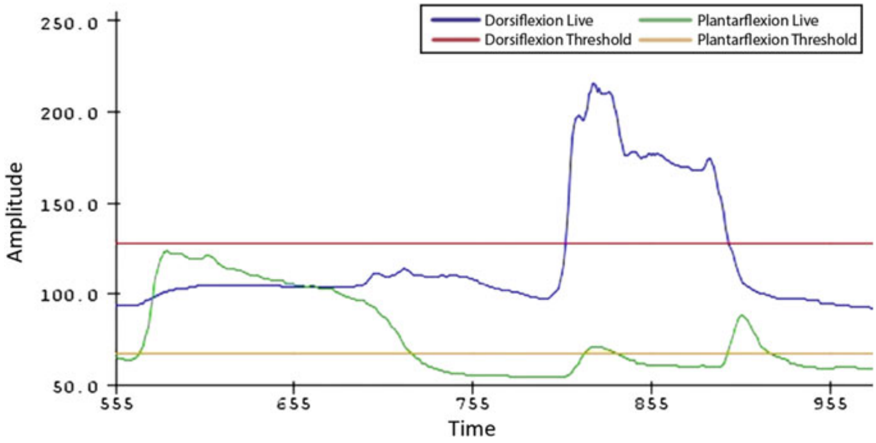


**Fig. 10** Voltage-time graph depicting filtered sensor data and the corresponding thresholds

**Fig. 11** Prototype of the ankle-foot orthosis

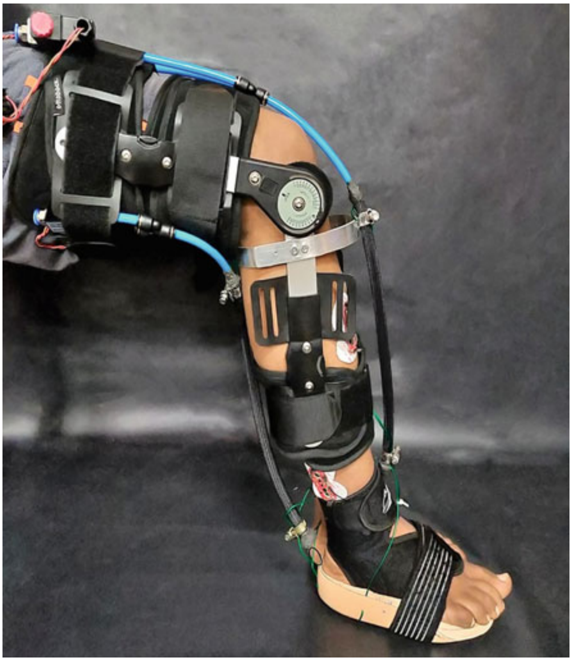

## 6 Conclusions

The design and control of a 1-DOF Soft Ankle-Foot Orthosis presented in this paper shows promise to be a therapeutic alternative for foot drop rehabilitation. The AFO uses EMG signals which are reliable and easy to calibrate. The main purpose of the work is to present the scope of soft-robotic devices as an alternative for rigid and heavy hardware previously used for robotic rehabilitation. The AFO uses PAMs, which are pneumatically actuated, low-cost and lightweight. The torque provided by the AFO can be increased by enhancing air pressure driving techniques, and this could allow the use of the device as an exoskeleton. Also, machine learning algorithms could be used to estimate the intent of the user with greater accuracy. The device could also be further developed by incorporating more degrees of freedom. This would allow the AFO to perform inversion and eversion of the leg.

## References

1. World Health Report—2002 from the World Health Organization Retrieved on: 2019 from http://www.who.int/whr/2002/en/
2. Walking abnormalities MedlinePlus Retrieved on: 2019 from https://medlineplus.gov/ency/article/003199.htm
3. Wiszomirska I, Błażkiewicz M, Kaczmarczyk K, Brzuszkiewicz-Kuźmicka G, Wit A (217) Effect of drop foot on spatiotemporal, kinematic, and kinetic parameters during gait. Appl Bionics Biomech. 2017:3595461. https://doi.org/10.1155/2017/3595461
4. Langhorne P, Bernhardt J, Kwakkel G (2011 ) Stroke rehabilitation, stroke care 2, The lancet, vol 377
5. Khor KX, Rahman HA, Fu SK et al (2014) A novel hybrid rehabilitation robot for upper and lower limbs rehabilitation training. In: Internatioinal conference on robot pride (ConfPRIDE) 2013–2014, procedia computer science, vol 42, pp 293–300
6. Asokan A, Vigneshwar M, Design and control of an EMG-based low-cost exoskeleton for stroke rehabilitation. In: 2019 fifth Indian control conference (ICC), New Delhi, India, pp 478–483. https://doi.org/10.1109/INDIANCC.2019.8715555
7. Kim B, Deshpande AD (2017) An upper-body rehabilitation exoskeleton harmony with an anatomical shoulder mechanism: design, modeling, control, and performance evaluation. Int J Rob Res (IJRR) 36(4):414–435
8. Perry JC, Rosen J, (26) Design of a 7 degree-of-freedom upper-limb powered exoskeleton. The First IEEE, RAS-EMBS Interenational conference on biomedical robotics and biomechatronics, (2006) BioRob 2006. Pisa 2006:805–810
9. Stroke rehabilitation: What to expect as you recover (2017) Retrieved on 2 June 2019, from https://www.mayoclinic.org/diseasesconditions/stroke/in-depth/stroke-rehabilitation/art-20045172
10. Ikuta K (1990) Micro/miniature shape memory alloy actuator. In: Proceedings IEEE international conference on robotics and automation, vol 3. Cincinnati, OH, USA, pp 2156–2161. https://doi.org/10.1109/ROBOT.1990.126323
11. Park Y-L, Chen B, Pérez-Arancibia NO, Young D, Stirling L, Wood RJ, Goldfield EC, Nagpal R (2014) Design and control of a bio-inspired soft wearable robotic device for ankle-foot rehabilitation. Bioinspiration Biomimetics 9(1). https://doi.org/10.1088/1748-3182/9/1/016007
12. Gordon KE, Sawicki GS, Ferris DP (2006) Mechanical performance of artificial pneumatic muscles to power an ankle-foot orthosis. J Biomech 39(10):1832–1841. https://doi.org/10.1016/j.jbiomech.2005.05.018

13. Arnez-Paniagua V, Rifai H, Amirat Y, Mohammed S (2017) Adaptive control of an actuated-ankle-foot-orthosis. In: 2017 International conference on rehabilitation robotics (ICORR). https://doi.org/10.1109/icorr.2017.8009474
14. Roy A, Krebs HI, Williams DJ, Bever CT, Forrester LW, Macko RM, Hogan N (2009) Robot-aided neurorehabilitation: a novel robot for ankle rehabilitation. IEEE Trans Rob 25(3):569–582. https://doi.org/10.1109/tro.2009.2019783
15. Banala SK, Kim SH, Agrawal SK, Scholz JP (2009) Robot assisted gait training with active leg exoskeleton (ALEX). IEEE Trans Neural Syst Rehabil Eng 17(1):2–8. https://doi.org/10.1109/tnsre.2008.2008280
16. Jakub T, Laski P, Slawomir B, Gabriel B, Dawid P (2016) Determining the static characteristics of pneumatic muscles. Measur Control 49:62–71. https://doi.org/10.1177/0020294016629176
17. Generally accepted values for normal range of motion (ROM) in joints (2019) Retrieved on 8 June 2019 from https://www.verywellhealth.com/what-is-normal-range-of-motion-in-a-joint-3120361
18. Ferris DP, Czerniecki JM, Hannaford B (2005) An ankle-foot orthosis powered by artificial pneumatic muscles. J Appl Biomech 21(2):189–197
19. Zhu Y (2017) Design and web-based control of a soft ankle foot orthosis 17:82–88
20. Appendicular Muscles of the Pelvic Girdle and Lower Limbs. Retrieved on 8 July 2019 from https://cnx.org/contents/FPtK1zmh@8.108:y9_gDy74@5/Appendicular-Muscles-of-the-Pelvic-Girdle-and-Lower-Limbs
21. Datasheet Retrieved on 8 June 2019 from https://cdn.sparkfun.com/datasheets/Sensors/Biometric/MyowareUserManualAT-04-001.pdf
22. De Luca CJ, Gilmore LD, Kuznetsov M, Roy SH (210) Filtering the surface EMG signal: movement artifact and baseline noise contamination. J Biomech 43(8):1573–1579. ISSN 0021-9290. https://doi.org/10.1016/j.jbiomech.2010.01.027
23. Muhammad J (2012) Signal acquisition using surface EMG and circuit design considerations for robotic prosthesis. In: Computational intelligence in electromyography analysis–a perspective on current applications and future challenges. https://doi.org/10.5772/52556
24. Reaz MBI, Hussain MS, Mohd-Yasin F (2006) Techniques of EMG signal analysis: detection, processing, classification and applications. Biol Proced Online 8(1):11–35
25. Özgunen KT, Çelik U, Kurdak SS (2010) Determination of an optimal threshold value for muscle activity detection in EMG analysis. J Sports Sci Med 9:620–628